Heterogeneous Catalysis

DOI: 10.1002/anie.201005275

A Flexible Nonporous Heterogeneous Catalyst for Size-Selective Oxidation through a Bottom-Up Approach**

Noritaka Mizuno, Sayaka Uchida, Keigo Kamata, Ryo Ishimoto, Susumu Nojima, Koji Yonehara, and Yasutaka Sumida*

The bottom-up approach has the potential to create novel devices with a wide range of applications such as in electronics, medicine, and energy, as the arrangement of molecular building blocks into nanostructures can be controlled.[1,2] It is still a great challenge to fabricate not only devices but also heterogeneous catalysts with intended structures and functions by a bottom-up approach,[3] while biominerals such as shells and bones have been already formed by the bottom-up approach through the self-assembly of inorganic building blocks with organic molecules in water.[4] The control of the self-organization of nanobuilding blocks with well-defined sizes, shapes, and physical and chemical properties would lead to progress in science and technology. Various catalytically active sites, such as metal nodes, framework nodes, and molecular species, can be introduced into metal–organic frameworks (MOFs) through self-assembly. Efficient size- and enantioselective catalysis by crystalline and porous MOFs has been reported for reduction, C–C bond formation, and acid–base reactions, and hydrolytic and oxidative stabilities are critical for the development of MOF-based oxidation systems that are efficient, chemo- and size-selective, and recyclable, and use the green oxidant H_2O_2.[5–7] Therefore, the development of efficient, easily recoverable, and recyclable heterogeneous oxidation catalysts with H_2O_2 by a bottom-up approach has received particular research interest.[3,8]

[*] Prof. Dr. N. Mizuno, Dr. S. Uchida, Dr. K. Kamata, R. Ishimoto, S. Nojima
Department of Applied Chemistry, School of Engineering, The University of Tokyo, Hongo, Bunkyo-ku, Tokyo 113-8656 (Japan)
Prof. Dr. N. Mizuno, Dr. S. Uchida, Dr. K. Kamata
Core Research for Evolutional Science and Technology (CREST) (Japan), Science and Technology Agency (JST), 4-1-8 Honcho, Kawaguchi, Saitama 332-0012 (Japan)
E-mail: tmizuno@mail.ecc.u-tokyo.ac.jp
Dr. K. Yonehara, Y. Sumida
Advanced Materials Research Center, Nippon Shokubai Co., Ltd., 5-8 Nishi Otabi-cho, Suita, Osaka 564-8512 (Japan)

[**] We are grateful to S. Kuzuya (The University of Tokyo) and M. Fujita (The University of Tokyo) for their help in experiments. This work was supported by the Core Research for Evolutional Science and Technology (CREST) program of the Japan Science and Technology Agency (JST), the Global COE Program (Chemistry Innovation through Cooperation of Science and Engineering), the Development in a New Interdisciplinary Field Based on Nanotechnology and Materials Science Programs, and a Grant-in-Aid for Scientific Research from the Ministry of Education, Culture, Science, Sports, and Technology of Japan.

Supporting information for this article is available on the WWW under http://dx.doi.org/10.1002/anie.201005275.

Polyoxometalates (POMs) are discrete early transition-metal oxide cluster anions with applications in broad fields, such as catalysis, materials, and medicine, because their structures and chemical properties can be finely tuned by choose of the constituent elements.[9–14] Various POMs such as peroxometalates, lacunary POMs, and transition-metal-substituted POMs have been developed for H_2O_2- or O_2-based green oxidations. Therefore, POMs are suitable nanobuilding blocks to construct heterogeneous oxidation catalysts. Recently, the development of heterogeneous oxidation catalysts based on POMs and the related compounds has been attempted according to the following strategies: "solidification" of POMs (formation of insoluble solid ionic materials with appropriate countercations) and "immobilization" of POMs through adsorption, covalent linkage, and ion exchange. In most cases, however, the catalytic activities and selectivities of the parent homogeneous POMs are somewhat or much decreased by the heterogenization, and there are only a few successful examples.[15–18] We are interested in a bottom-up approach to the design and synthesis of artificial heterogeneous catalysts with POMs and herein report that the nonporous tetra-*n*-butylammonium salt of $[\gamma\text{-}SiW_{10}O_{34}(H_2O)_2]^{4-}$ ($[(n\text{-}C_4H_9)_4N]_4[\gamma\text{-}SiW_{10}O_{34}(H_2O)_2]\cdot H_2O$, **1·H$_2$O**) synthesized through a bottom-up approach sorbs ethyl acetate (EtOAc), which is highly mobile in the solid bulk of the compound, probably contributing to the easy co-sorption of the olefins and H_2O_2. The compound heterogeneously catalyzes size-selective oxidation of various organic substances including olefins, sulfides, and silanes with aqueous H_2O_2 in EtOAc. The compound can easily be separated by filtration and reused several times with retention of its high catalytic activity. The catalysis is truly heterogeneous in nature because the filtrate after removal of the solid catalyst is completely inactive. Notably, size-selective oxidation catalysis is observed: small olefins are much more preferentially epoxidized than large olefins. To the best of our knowledge, this study provides the first example for the heterogeneously catalyzed size-selective liquid-phase oxidation with H_2O_2 by a POM-based catalyst.

Compound **1·H$_2$O** was synthesized by a bottom-up approach as described below. The silicodecatungstate $[\gamma\text{-}SiW_{10}O_{34}(H_2O)_2]^{4-}$ was synthesized in situ by the addition of concentrated HNO_3 to an aqueous solution of $[\gamma\text{-}SiW_{10}O_{36}]^{8-}$. Then, tetra-*n*-butylammonium bromide $[(n\text{-}C_4H_9)_4N]\cdot Br$ was added to the solution, and white powder of **1·H$_2$O** was formed.[19] The use of other cations, such as tetramethylammonium $[(CH_3)_4N]^+$, formed single crystals.[19] The powder X-ray diffraction (XRD) pattern, crystal structure, and space-filling model of **1·H$_2$O** are shown in Figure 1 a–c. The

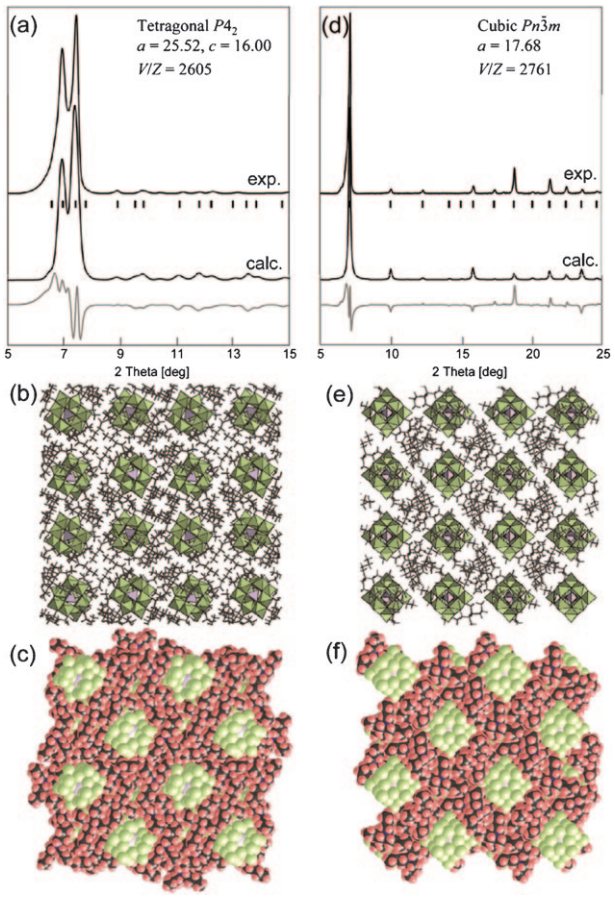

Figure 1. a) Experimental and calculated powder XRD patterns, b) crystal structure, and c) space-filling model of **1·H₂O**. d) Experimental and calculated powder XRD patterns, e) crystal structure, and f) space-filling model of **1·EtOAc**. Gray lines and black markers in (a) and (d) show the differences between the experimental and calculated data and the calculated peak positions, respectively. Light green and purple polyhedra in (b) and (e) show the $[WO_6]$ and $[SiO_4]$ units, respectively. Black sticks in (b) and (e) show the $[(n\text{-}C_4H_9)_4N]^+$ fragments. Light green spheres in (c) and (f) show the tungsten and oxygen atoms of $[\gamma\text{-}SiW_{10}O_{34}(H_2O)_2]^{4-}$. Purple, dark gray, and pink spheres in (c) and (f) show the silicon, carbon, and hydrogen atoms, respectively.

calculated peak positions and shapes agreed fairly well those found experimentally (Figure 1 a). The rather large difference between the experimental and calculated data, especially at higher angles, is probably because of the variations of electron densities in the unit cell, which may be caused by the highly disordered alkyl chains of the tetra-*n*-butylammonium cations. Therefore, the tetra-*n*-butylammonium cations were not located with the powder XRD analysis but with the molecular mechanics using a universal force field. In the crystal lattice of **1·H₂O**, the $[\gamma\text{-}SiW_{10}O_{34}(H_2O)_2]^{4-}$ ions were arranged in a tetragonal cell and surrounded by the $[(n\text{-}C_4H_9)_4N]^+$ cations. The constituent ions were densely packed in the unit cell, and **1·H₂O** was nonporous with a normalized unit cell volume (V/Z) of 2605 Å^3. The water of crystallization in **1·H₂O** was desorbed by the evacuation or treatment with dry He gas flow at 298–333 K to form the guest free phase $[(n\text{-}C_4H_9)_4N]_4[\gamma\text{-}SiW_{10}O_{34}(H_2O)_2]$ (**1**). The powder XRD pattern of **1** was similar to that of **1·H₂O**, indicating that the structure is maintained after desorption of the water of crystallization (Figure S1 in the Supporting Information). The surface area of **1** calculated with the Brunauer–Emmett–Teller (BET) plot of the N_2 adsorption isotherm (77 K, Figure S2) was 5.4 $m^2 g^{-1}$ and low, which agreed with the nonporous crystal structure of **1**. In addition, the particle size of **1** calculated with the BET surface area (5.4 $m^2 g^{-1}$) and density (2.17 $g cm^{-3}$) assuming spherical particles was $r = 0.26$ μm, and agreed fairly well with the SEM image ($r = 0.25$ μm) of **1**.

Compound **1** could act as an effective heterogeneous catalyst for the oxidation of 1-hexene with H_2O_2 in insoluble EtOAc to give 1,2-epoxyhexane in 92% yield. The epoxidation of 1-hexene was completely stopped by the removal of **1** from the reaction solution (Figure S3). In addition, it was confirmed by inductively coupled plasma atomic emission spectroscopy that the tungsten content in the filtrate was less than 0.2% of that in fresh **1**. These results indicate that any tungsten species that leached into the reaction solution is not an active homogeneous catalyst and that the observed catalysis is truly heterogeneous in nature. The epoxidation did not proceed efficiently without EtOAc, suggesting that EtOAc promotes the present heterogeneous oxidation catalysis. Compound **1** sorbed $(4.4 \pm 0.4) \times 10^{-1}$ mol mol^{-1} of 1-hexene from the mixture with EtOAc, and the amount was two orders of magnitude larger than that of the surface adsorption (ca. 4.0×10^{-3} mol mol^{-1}) [Eq. (1)]. Compound **1** sorbed 2.3 ± 0.1 mol mol^{-1} H_2O_2 from the mixture with EtOAc [Eq. (2)]. These results show that both reactant and oxidant are sorbed into the solid bulk of **1** by the presence of EtOAc.

$$\mathbf{1}\ (0.5\ \text{g}) \xrightarrow[\text{EtOAc (6 mL)}]{\text{1-hexene (2 mmol)}} \mathbf{1} \bullet (4.4 \pm 0.4) \times 10^{-1}\ \text{1-hexene} \qquad (1)$$
333 K, 3 h

$$\mathbf{1}\ (0.125\ \text{g}) \xrightarrow[\text{EtOAc (3 mL)}]{\text{60\% } H_2O_2\ (0.5\ \text{mmol})} \mathbf{1} \bullet 2.3 \pm 0.1\ H_2O_2 \qquad (2)$$
333 K, 3 min

$$I(t) = I_0(1 - T_{CH}/T_{1\rho(H)})^{-1}\ \{\exp(-t/T_{1\rho(H)}) - \exp(-t/T_{CH})\} \qquad (3)$$

The powder XRD pattern of **1** (Figure 1 a) was completely changed by EtOAc sorption (Figure 1 d). The structure analyses of the powder XRD patterns showed that the crystal system changed from tetragonal to cubic and the cell volume (V/Z) increased from 2605 Å^3 to 2761 Å^3 with EtOAc sorption. The increase in the cell volume (156 Å^3) agreed well with the volume of the EtOAc molecule (162 Å^3) calculated from the molecular weight and density of the liquid, suggesting that 1 mol mol^{-1} of EtOAc was sorbed into the crystal lattice of **1**.

During the spin locking step in ^{13}C cross-polarization magic-angle spinning (CPMAS) NMR spectroscopy, there is magnetization transfer from ^1H to ^{13}C through heteronuclear dipolar interactions. The cross-polarization process is described by Equation (3) with an assumption $T_{CH} \ll T_{1\rho(H)}$, where $I(t)$, I_0, T_{CH}, and $T_{1\rho(H)}$ represent the intensity of the signal at contact time of t, theoretical maximum intensity of

the signal, cross-polarization time constant, and proton spin-lattice relaxation time, respectively.[20,21]

As a result, the signal intensity of the less mobile carbon atom reaches a maximum at relatively short contact times (shorter T_{CH}). Therefore, the mobilities of the $[(n\text{-}C_4H_9)_4N]^+$ cations of **1** as a host and EtOAc molecules as a guest were investigated with variable contact time CPMAS NMR spectroscopy. The changes in the ^{13}C CPMAS NMR spectra of **1·EtOAc** at 333 K with an increase in contact times are shown in Figure S4. In the range of short contact times ($\leq$5 ms), only the signals for the C1–C4 carbon atoms of $[(n\text{-}C_4H_9)_4N]^+$ were observed. At a contact time of 10 ms, the signals for $[(n\text{-}C_4H_9)_4N]^+$ almost disappeared and those for EtOAc appeared. In the range 10–100 ms, the intensities of the signals for EtOAc monotonically increased. The cross-polarization time constants for the C1, C2, C3, and C4 carbon atoms of $[(n\text{-}C_4H_9)_4N]^+$ were 0.11, 0.12, 0.16, and 0.22 ms, respectively (Figure 2). These values are comparable to those

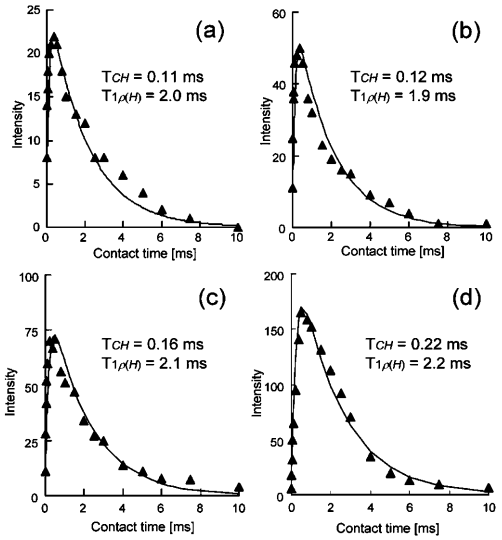

Figure 2. Peak intensities of the ^{13}C CPMAS NMR spectra of **1·EtOAc** at 333 K as a function of contact time. a) C1 (δ = 57.9 ppm), b) C2 (δ = 24.6 ppm), c) C3 (δ = 20.3 ppm), and d) C4 (δ = 14.9 ppm) of $(n\text{-}C_4H_9)_4N^+$.

of the alkylammonium surfactants in mesoporous silica.[22] Notably, the cross-polarization time constants for the carbon atoms of EtOAc were approximately 60 ms and much longer, suggesting high mobility of the EtOAc molecules (Figure 3).

The epoxidation of nonactivated propene in EtOAc with H_2O_2 catalyzed by **1** also proceeded efficiently to form 1,2-epoxypropane in 89% yield (Figure 4). After the epoxidation, **1** could easily be separated from the reaction mixture by simple filtration. The recovered **1** after the epoxidation could be reused at least four times without significant loss of catalytic activity (95% (1st reuse), 86% (2nd reuse), and 91% (3rd reuse)). In addition, the present system could be applied to the heterogeneous and recyclable oxidation of ethylpropylsulfide and ethyldimethylsilane to the corresponding sulfoxide and silanol (Figure 4). 1,2-Epoxybutane was obtained in 90% yield with 90% selectivity in a 240 mmol

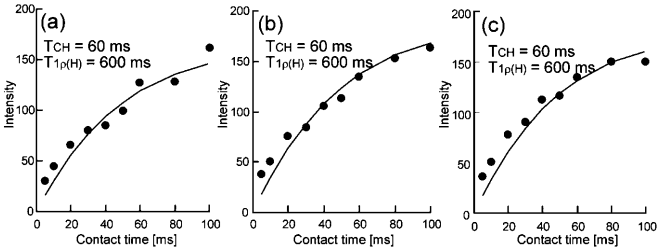

Figure 3. Peak intensities of the ^{13}C CPMAS NMR spectra of **1·EtOAc** at 333 K as functions of contact time. a) Methylene group (δ = 60.0 ppm), b) methyl group of acetate moiety (δ = 20.0 ppm), and c) methyl group of ethoxy moiety (δ = 14 ppm).

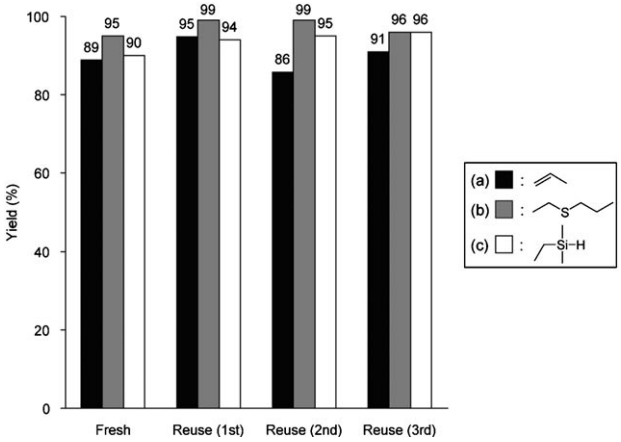

Figure 4. Recycling of **1** for the oxidation of a) propene, b) ethylpropylsulfide, and c) ethyldimethylsilane. Reaction conditions: a) **1** (2 mol%), propene (6 atm), 60% H_2O_2 (1 mmol), EtOAc (6 mL), 333 K, 3 h. b) **1** (0.7 mol%), ethylpropylsulfide (3 mmol), 60% H_2O_2 (1 mmol), EtOAc (3 mL), 313 K, 2 h. c) **1** (2 mol%), ethyldimethylsilane (3 mmol), EtOAc (6 mL), 333 K, 3 h.

scale epoxidation of 1-butene with H_2O_2 in the butyl acetate solvent, and the retention of high catalytic performance in a large-scale epoxidation raises the prospect of the present system for the industrial heterogeneous epoxidation [Eq. (4)]. Since the reaction rates for the heterogeneous system were smaller than those for the homogeneous one, longer reaction times were needed. In addition, the heterogeneous system required higher reaction temperature than the homogeneous system (especially for the larger olefins). Therefore, non-productive decomposition of H_2O_2 proceeds in some cases, resulting in a slight decrease in yields for the present heterogeneous system.

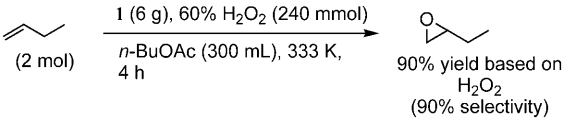

(4)

Notably, the size-selective heterogeneous epoxidation proceeded with **1** in EtOAc, while no size-selectivity was observed for the **1**-catalyzed homogeneous competitive epoxidation in acetonitrile in accord with the π(C=C)

HOMO energies (Table S1). In the case of the heterogeneous competitive epoxidation of 1-hexene and various C3–C12 terminal olefins, the yield ratios of the C3–C12 epoxides to 1,2-epoxyhexane monotonically decreased to 0.04 with an increase in the molecular cross-sectional areas of the C3–C12 olefins (Figure 5). The amounts of 1-hexene and 1-dodecene

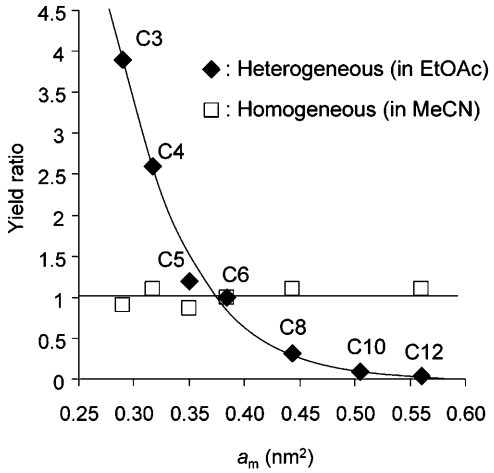

Figure 5. Plots of the ratios of the C3–C12 epoxides to 1,2-epoxyhexane for competitive epoxidation of various C3–C12 terminal olefins and 1-hexene against the molecular cross-sectional areas of the olefins. The details are shown in Table S1.

sorption from a mixture in EtOAc were $(4.4 \pm 0.8) \times 10^{-1}$ and $(4.0 \pm 3.0) \times 10^{-2}$ mol mol^{-1}, respectively [Eq. (5)], which is in accord with the much faster epoxidation of 1-hexene than 1-dodecene in Figure 5. The yield ratios of the C3–C12 epoxides to 1,2-epoxyhexane against the molecular cross-sectional areas of the C3–C12 olefins for the heterogeneous competitive epoxidation of 1-hexene and various C3–C12 terminal olefins in the presence of $[(n\text{-}C_5H_{11})_4N]_4[\gamma\text{-}SiW_{10}O_{34}(H_2O)_2]$ monotonically decreased to 0.05 with an increase in the molecular cross-sectional areas in a similar way to that of $[(n\text{-}C_4H_9)_4N]_4[\gamma\text{-}SiW_{10}O_{34}(H_2O)_2]$ (Figure S5). Therefore, the size-selectivity was not much changed by the change of the counter cation from $[(n\text{-}C_4H_9)_4N]^+$ to $[(n\text{-}C_5H_{11})_4N]^+$.

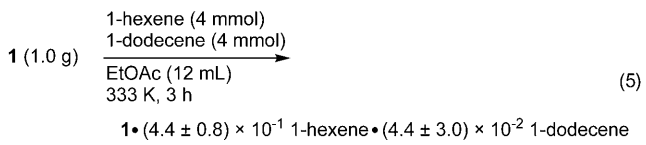

The ratio of C8 epoxide to C6 epoxide for the competitive epoxidation of 1-hexene and 1-octene remained almost unchanged as a function of time (Figure S6), suggesting little variation in the size-selectivity during the epoxidation. In addition, the ratios of C8 epoxide to C6 epoxide varied little with changes in the size and dipole moment of solvents (Figure S7).

The reactivity for the heterogeneous and homogeneous epoxidation of a series of C6 olefins catalyzed by **1** are shown in Table S2. The reactivity order was different from each other. In the heterogeneous system, the reaction rates for the terminal olefins were increased with respect to those for the branched olefins. Such an order was also observed for epoxidation catalyzed by TS-1 (titanium silicalite), for which restricted transition-state shape selectivity and diffusion effects were observed.[23] In addition, the competitive epoxidation of propene and cyclododecene gave 1,2-epoxypropane and 1,2-epoxycyclododecane in 66% and 14% yields, respectively, whereas 1,2-epoxycyclododecane was obtained preferentially in the homogeneous system [Eq. (6)]. Not only olefins but also sulfides (ethylpropylsulfide vs. dibutylsulfide) and silanes (ethyldimethylsilane vs. tripropylsilane) were oxidized size-selectively in EtOAc solvent [Eqs. (7) and (8)] and the small substrates were preferentially oxidized to the corresponding sulfoxide and silanol. Since the EtOAc molecules are highly mobile in the solid bulk of **1**, it is probable that the sorption of olefins and H_2O_2 and the size-selectivity is largely enhanced by its presence. Such a unique sorption property of **1** resulted in heterogeneous, recyclable, and size-selective epoxidation catalysis with H_2O_2. To the best of our knowledge, size-selective oxidation catalyzed by POM-based compounds has never been reported to date.

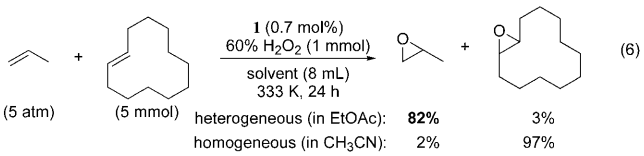

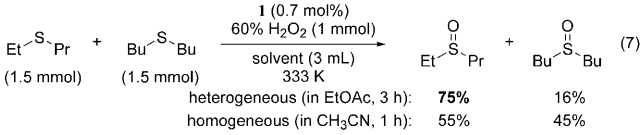

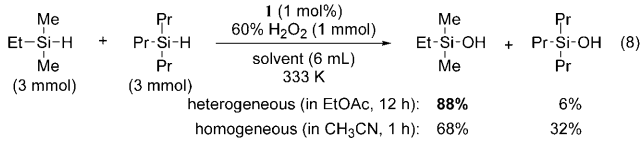

Received: August 24, 2010
Published online: November 17, 2010

Keywords: heterogeneous catalysis · oxidation · polyoxometalates · size-selectivity · structure elucidation

[1] W. Lu, C. M. Lieber, *Nat. Mater.* **2007**, *6*, 841–850.
[2] H. Cölfen, M. Antonietti, *Angew. Chem.* **2005**, *117*, 5714–5730; *Angew. Chem. Int. Ed.* **2005**, *44*, 5576–5591.
[3] W. Schmidt, *ChemCatChem* **2009**, *1*, 53–67.
[4] J. D. Hartgerink, E. Beniash, S. I. Stupp, *Science* **2001**, *294*, 1684–1688.
[5] A. Corma, H. García, F. X. Llabrés i Xamena, *Chem. Rev.* **2010**, *110*, 4606–4655.
[6] J. Y. Lee, O. K. Farha, J. Roberts, K. A. Scheidt, S. B. T. Nguyen, J. T. Hupp, *Chem. Soc. Rev.* **2009**, *38*, 1450–1459.

[7] L. Alaerts, J. Wahlen, P. A. Jacobs, D. E. De Vos, *Chem. Commun.* **2008**, 1727 – 1737.
[8] R. A. Sheldon, M. C. A. van Vliet, *Fine Chemicals through Heterogeneous Catalysis*, Wiley-VCH, Weinheim, **2001**.
[9] R. Neumann, *Prog. Inorg. Chem.* **1998**, *47*, 317 – 370.
[10] *Special Thematic Issue on Polyoxometalates* (Ed.: C. L. Hill), *Chem. Rev.* **1998**, *98*, 1 – 390.
[11] I. V. Kozhevnikov, *Catalysts for Fine Chemical Synthesis: Catalysis by Polyoxometalates*, Wiley, Chichester, **2002**.
[12] M. T. Pope in *Comprehensive Coordination Chemistry II*, *Vol. 4* (Eds.: J. A. McCleverty, T. J. Meyer), Elsevier Pergamon, Amsterdam, **2004**, pp. 635 – 678.
[13] C. L. Hill in *Comprehensive Coordination Chemistry II*, *Vol. 4* (Eds.: J. A. McCleverty, T. J. Meyer), Elsevier Pergamon, Amsterdam, **2004**, pp. 679 – 758.
[14] N. Mizuno, K. Kamata, S. Uchida, K. Yamaguchi in *Modern Heterogeneous Oxidation Catalysis* (Ed.: N. Mizuno), Wiley-VCH, Weinheim, **2009**, pp. 185 – 216.
[15] J. T. Rhule, W. A. Neiwert, K. I. Hardcastle, B. T. Do, C. L. Hill, *J. Am. Chem. Soc.* **2001**, *123*, 12101 – 12102.
[16] K. Yamaguchi, C. Yoshida, S. Uchida, N. Mizuno, *J. Am. Chem. Soc.* **2005**, *127*, 530 – 531.
[17] R. Neumann, H. Miller, *J. Chem. Soc. Chem. Commun.* **1995**, 2277 – 2278.
[18] B. Sels, D. De Vos, M. Buntinx, F. Pierard, A. Kirsch-De Mesmaeker, P. Jacobs, *Nature* **1999**, *400*, 855 – 857.
[19] K. Kamata, K. Yonehara, Y. Sumida, K. Yamaguchi, S. Hikichi, N. Mizuno, *Science* **2003**, *300*, 964 – 966.
[20] C. A. Fyfe, A. C. Diaz, H. Grondey, A. R. Lewis, H. Forster, C. A. Jyfe, *J. Am. Chem. Soc.* **2005**, *127*, 7543 – 7558.
[21] S. H. Liang, I. D. Gay, *Langmuir* **1985**, *1*, 593 – 599.
[22] L. Q. Wang, J. Liu, G. J. Exarhos, B. C. Bunker, *Langmuir* **1996**, *12*, 2663 – 2669.
[23] M. G. Clerici, P. Ingallina, *J. Catal.* **1993**, *140*, 71 – 83.

